Large Eddy Simulation of Swirling Turbulent Jet Flows

Celestin P. Zemtsop, Michael K. Stoellinger, Stefan Heinz, and Dan Stanescu

Department of Mathematics, University of Wyoming
1000 East University Avenue, Laramie, WY 82071, USA

Email:*czemtsop@uwyo.edu*

ABSTRACT

The paper reports the results of numerical investigations of swirling turbulent jet flows by large eddy simulation (LES). Inflow data are provided on the basis of Reynolds-averaged Navier-Stokes (RANS) simulations. In particular, instantaneous inflow data are produced by a forcing that generates correlated noise. In this way, the characteristic length and time scales of inflowing instantaneous turbulent eddies are in consistency with the corresponding RANS profiles imposed at the inlet. The performance of several subgrid-scale stress models is studied. The mechanism of swirl effects is investigated on this basis. It is shown that swirl increases streamwise braid structures which enhance the breakdown of the characteristic ring-like structures in round jets. It is shown that swirl implies an increase of the efficiency of the turbulent mixing of scalars.

1. INTRODUCTION

Improving the efficiency of turbulent jet mixing can produce several performance enhancements for aircrafts including decreased jet noise, lower plume temperatures, increased combustion efficiency and reduced pollutant emission. One proven mixing enhancement approach is the use of swirl, which is known to enhance jet growth rates due to changes in the jet turbulence [1, 2]. Numerical simulations can provide a deep insight into the mechanism of swirling turbulent jets. Reynolds-averaged Navier-Stokes (RANS) methods represent the most efficient methodology for the calculation of turbulent flows, but the use of standard RANS methods for swirling jet flow simulations turned out to be inappropriate [3]. Large eddy simulation (LES) has been proven to be an accurate and computationally feasible approach for turbulent swirl flow simulations [4].

However, there are several relevant questions regarding the realization and interpretation of turbulent swirl flow LES. The inflow conditions of such jet flows are often determined by a nozzle flow, and experimental investigations of flow fields at nozzle exits often provide incomplete information about inflow data for turbulent swirl flow LES. For example, the dissipation rate of turbulent kinetic energy is hardly measurable such that measurements cannot provide information about the typical length and time scales of inflowing eddies. One way to obtain information required to determine the inflow data for jet simulations is to perform a LES of the nozzle flow. However, this approach turns out to be too expensive computationally. Thus, nozzle flow simluations have to be performed on the basis of RANS simulations. This approach involves the need for a forcing that generates instantaneous inflow data. However, the relevance and optimal generation of such forcing are still unclear [4, 5, 6, 7]. There are also several questions regarding the interpretation of LES data to identify coherent structures and swirl effects. For example, it is unclear right now how coherent structures can be analyzed in an optimal way, this mean which variables should be considered [4, 8, 9].

The questions discussed in the preceding paragraph will be addressed here. The flows considered will be described in section 2. Sections 3 and 4 describe the generation of LES inflow data and realization of LES, respectively. A comparison of averaged LES results with available experimental data is provided in section 5. These comparisons are used to evaluate the relevance of the forcing applied and the suitability of several subgrid-scale (SGS) stress models. Section 6 deals with an investigation of swirl effects by analyzing instantaneous LES data. Finally, section 7 summarizes the results reported here.

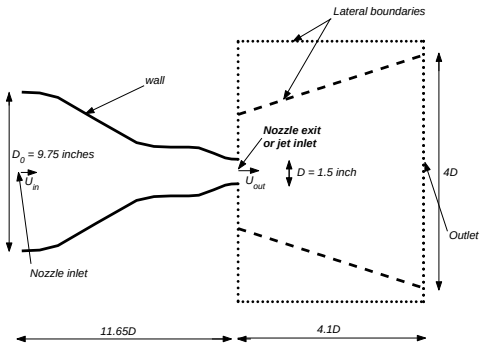

Figure 1: Nozzle design and jet region considered. The solid line refers to the nozzle body. The nozzle is $11.65D$ long. $D = 1.5$ in is the nozzle diameter at the exit and $D_0 = 9.75$ in is the nozzle diameter at the inlet. The jet region considered is $4.1D$ long. The solid and dotted lines represent the computational domain for the nozzle flow simulations. The conical dashed lines determine the computational domain for the jet flow simulations.

Table 1: Numerical setup for the LES jet flows

Simulations tools	Settings
Domain	3-dimensional: Conic with length 4.1D, radius 1D, 2D; divided into $370,000$ cells.
Solver	Pressure based
SGS models	DSM [12] with $0 \leq C_s \leq 0.23$ SSM [13] with $C_s = 0.17$ DKEM [14]
Method	Finite volume
Discretization	Bounded central differencing for momentum [15]; SIMPLEC for pressure-velocity coupling

2. THE FLOWS CONSIDERED

The effect of different swirl distributions has been investigated experimentally by Gilchrist and Naughton [10]. These investigations revealed significant changes in growth rates, turbulence intensities and the turbulence structures if swirl was added to the flow. These modifications have been attributed to centrifugal instabilities [11]. The geometry of the nozzle and jet flows considered are illustrated in figure 1. Two different swirl profiles have been investigated in the study of Gilchrist and Naughton [10]: one resembling a q-vortex (solid-body core with a free vortex outer region) and the other resembling a solid-body rotation. To generate these different swirl profiles, Gilchrist and Naughton used a unique facility which allows for fine control of the tangential velocity profile and the creation of a swirling jet that is largely free from artifacts produced by the swirl generation process [10]. For both vortex types measurements of the mean quantities and turbulence statistics are available for swirl numbers S = 0.1 and S = 0.23 at a jet Reynolds number $Re = 1.0 \times 10^5$. Corresponding data for a non-swirling case are also available. Here, only the non-swirling case and the solid-body swirling case with the swirl number S = 0.23 are considered for comparisons.

Although relevant conclusions could be obtained from the experiments of Gilchrist and Naughton [10], many important questions have yet to be clarified. For example, important information for the understanding of turbulent flows is given by the characteristic time and length scales of turbulent eddies. To obtain the turbulence time and length scales one needs to know the dissipation rate of turbulent kinetic energy. Unfortunately, it is extremely difficult to accurately measure this quantity. Thus, the only way to obtain the needed information on the turbulence scales is given by numerical studies of turbulent swirling jet flows.

3. LES INFLOW SIMULATIONS

To simulate the flows described in section 2, one needs inflow data for the jet simulations. Unfortunately, experimental data obtained at the nozzle exit do not provide sufficient information to determine the jet inflow conditions. To account correctly for the jet inflow conditions, the best way would be given by a LES of both the nozzle and jet flows. However, this approach turns out to be infeasible because of the huge computational cost for LES of the wall-bounded nozzle flow [16]. A way to overcome this problem is to use a combination of RANS and LES methods. RANS simulations are performed to simulate the flow within the nozzle. The profiles of the mean flow variables and turbulence statistics obtained by these RANS simulations are then used as inlet conditions for a LES of the region downstream of the nozzle exit.

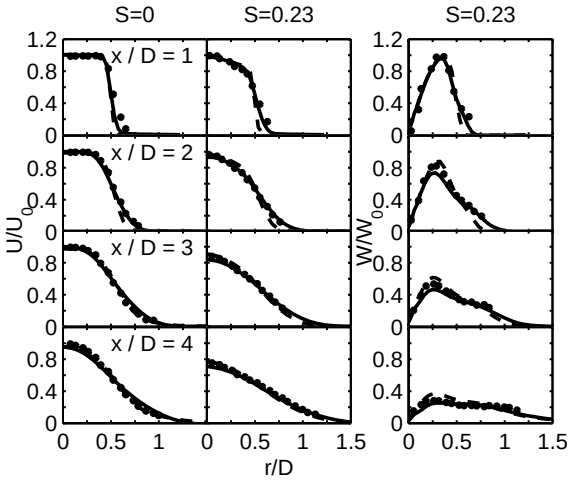

Figure 2: Radial distributions of the normalized averaged axial velocity U and tangential velocity W for the swirl number $S = 0$ case and the swirl number $S = 0.23$ solid body case at different axial positions x / D. The solid lines refer to forced LES results, dashed lines refer to the results of the no-perturbation LES, and dots denote the experimental data of Gilchrist and Naughton [10]. The normalization data are $U_0 = 50.4m/s$ for the non-swirling case, $U_0 = 56.3m/s$ and $W_0 = 21.7m/s$ for the swirling case.

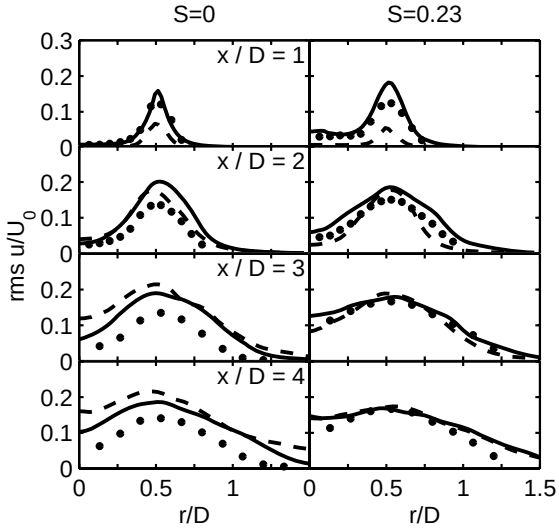

Figure 3: Radial distributions of normalized averaged intensities rms u of axial velocity fluctuations for the swirl number $S = 0$ and the swirl number $S = 0.23$ cases at different axial positions x / D. The solid lines refer to forced LES results, dashed lines refer to the results of the no-perturbation LES, and dots denote the experimental data of Gilchrist and Naughton [10]. The normalization data are $U_0 = 50.4m/s$ for the non-swirling case and $U_0 = 56.3m/s$ for the swirling case.

Several standard turbulence models were used to perform nozzle flow RANS simulations, but only the shear-stress transport (SST) $k-\omega$ model [17] provided acceptable results. The RANS simulations were performed on the basis of the FLUENT code [15]. The nozzle flow RANS simulations were shown to be in a very good agreement with the experimental data at the nozzle exit. It was also shown that the RANS method applied is inappropriate to perform simulations of the region downstream of the jet exit: RANS predictions obtained in this way disagree significantly with the experimental data. The latter observation agrees with the findings of Jakirlic et al. [3].

The results of RANS simulations described in the preceding paragraph were used as inflow data for LES of the jet flows. A significant problem related to LES of swirling turbulent jets is given by the need for fluctuating inflow data [6, 7]. Thus, a forcing mechanism was applied to produce fluctuating velocities at the inlet based on RANS results. In particular, the random flow generation (RFG) technique of Smirnov et al. [5] was used. This method represents a modification of the technique proposed originally by Kraichnan [18]. The advantage of this technique is given by the generation of correlated noise [19, 20] such that the characteristic length and time scales of inflowing instantaneous turbulent eddies are in consistency with the corresponding RANS profiles imposed at the inlet. The time dependent fluctuating velocities generated by the RFG method were added to the mean velocity profiles computed by the RANS method. In addition to the forced LES, a LES with non-fluctuating inlet conditions was performed (the no-perturbation case).

4. JET FLOW LES

Several SGS stress models required to close the LES equations were applied: the dynamic Smagorinsky model (DSM) [12], the standard Smagorinsky model (SSM) [13] with a Smagorinsky constant C_s = 0.17, and the dynamic kinetic energy model (DKEM) [14]. The inflow boundary conditions for velocities are described in section 3. A pressure-inlet boundary condition was used for lateral boundaries, and a pressure-

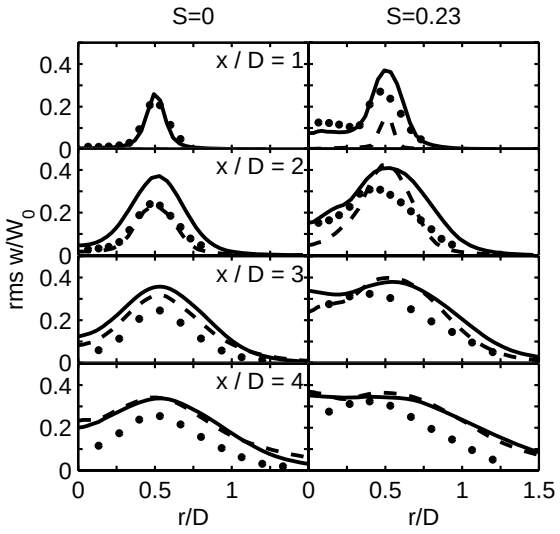

Figure 4: Radial distributions of normalized averaged intensities rms w of azimuthal velocity fluctuations for the swirl number $S = 0$ and the swirl number $S = 0.23$ case at different axial positions x / D. The solid lines refer to forced LES results, dashed lines refer to the results of the no-perturbation LES, and dots denote the experimental data of Gilchrist and Naughton [10]. The normalization is given by $W_0 = 21.7m/s$.

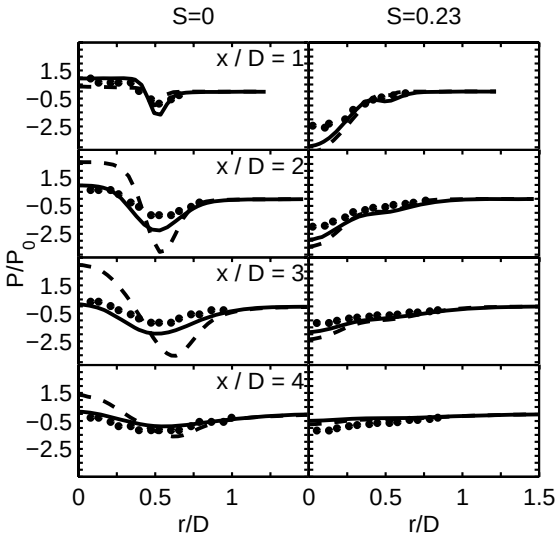

Figure 5: Radial distributions of the normalized averaged static pressure P for the swirl number $S = 0$ and the swirl number $S = 0.23$ case at different axial positions x / D. The solid lines refer to forced LES results, dashed lines refer to the results of the no-perturbation LES, and dots denote the experimental data of Gilchrist and Naughton [10]. The normalization data are P_0 = 23 Pa for the non-swirling case and P_0 = 94 Pa for the swirling case.

outlet boundary condition was used for the outlet boundary. The transport of a passive scalar was also considered to illustrate the modifications of turbulent mixing due to swirl. An eddy diffusivity model was employed to account for the SGS contribution with a turbulent Schmidt number of 1. The scalar is equal to 1 at the jet inlet and 0 otherwise at the inlet. The scalar value was set to 0 at the lateral boundaries, and zero gradient boundary conditions are applied at the outlet.

The computational domain is conical with a radius of $1D$ and $2D$ at the inlet and outlet, respectively. The domain extends up to $4.1D$ downstream (see figure 1). The domain is discretized into 80 points in azimuthal direction (uniformly distributed), 60 points in the radial direction (uniformly distributed) and 80 points in the axial direction with a stretching of 2%. The incompressible LES equations have been solved by a finite volume method based on the CFD code FLUENT [15]. Bounded central differencing is used for the spatial discretization of the momentum equations, a second-order upwind scheme is used for the spatial discretization of the passive scalar equation, and time is advanced via a second-order accurate implicit scheme. The SIMPLEC method is used for the pressure-velocity coupling. Details of the numerical setup are summarized in table 1.

The simulations were run for 15 large eddy turnover times $t_e = D/U_0$ to eliminate effects of the initial conditions. After this time, the simulations were run for another 920 large eddy turnover times to collect time statistics. Samples are taken every 5^{th} time step giving a total of $2,500$ samples. Due to the axi-symmetry of the flow an additional averaging of the time statistics over 80 points in the azimuthal direction has been performed. All averages referred to in this paper have been obtained by this method. All the simulations have been performed on 12 processors of a Beowulf LINUX cluster provided and operated by the Institute of Scientific Computation (ISC) at the University of Wyoming. Obtaining the necessary time statistics required a computational time of about 72 hours.

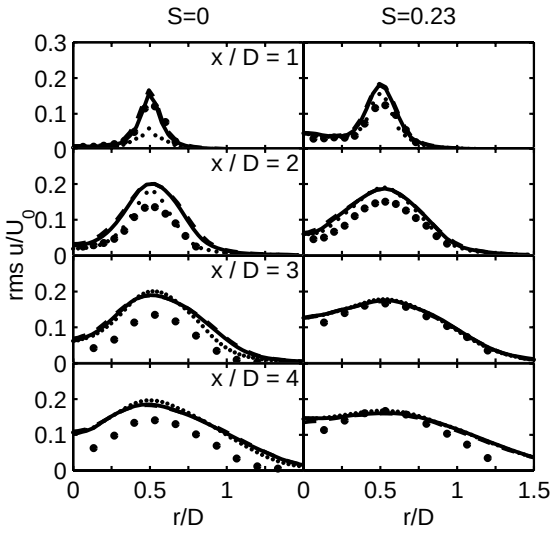

Figure 6: Radial distributions of normalized averaged intensities rms u of axial velocity fluctuations for the $S = 0$ and $S = 0.23$ cases at different axial positions x / D. The solid lines refer to results of forced LES with the DSM, dashed lines refer to results with the DKEM, little dots refer to results with the SSM, and dots denote the experimental data of Gilchrist and Naughton [10]. Here, $U_0 = 50.4m/s$ for the non-swirling case and $U_0 = 56.3m/s$ for the swirling case.

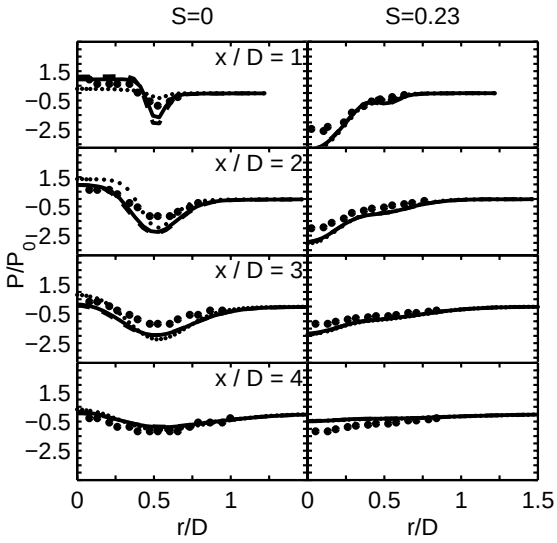

Figure 7: Radial distributions of normalized averaged static pressure P for the $S = 0$ and $S = 0.23$ cases at different axial positions x / D. The solid lines refer to results of forced LES with the DSM, dashed lines refer to results with the DKEM, little dots refer to results with the SSM, and dots denote the experimental data of Gilchrist and Naughton [10]. The normalization data are P_0 = 23 Pa for the non-swirling case and P_0 = 94 Pa for the swirling case.

5. FORCING AND SGS EFFECTS

The effects of forcing and SGS modeling were investigated by comparing averaged flows fields with experimental data [10]. The simulation results for the forced LES and no-perturbation LES combined with the DSM for the SGS stress are shown in figures 2, 3, 4, and 5. The non-swirling and swirling solid-body rotation cases are compared in these figures at different downstream positions. In particular, figure 2 shows the radial distribution of the normalized averaged axial velocity U/U_0 and the normalized averaged azimuthal velocity W/W_0, figure 3 shows the intensity rms u/U_0 of axial velocity fluctuations, figure 4 shows the intensity rms w/W_0 of azimuthal velocity fluctuations, and figure 5 shows the averaged static pressure P/P_0. The mean axial and azimuthal velocities are well represented by the forced LES. There is a minor overprediction of the intensities of axial and tangential velocity fluctuations. Also, a minor underprediction of the static pressure is observed. The lack of forcing implies a significant underprediction of axial velocity fluctuations at x/D = 1. Hence, the jet expansion is underpredicted: see the results for axial velocities. The latter implies steeper mean velocity gradients which produce more turbulence. Therefore, the intensity of axial velocity fluctuations increases strongly which leads to the overprediction observed at x/D = 3, and x/D = 4. Thus, the inclusion of forcing has a positive effect.

Results of simulations adopting the DSM, the DKEM, and the SSM for the SGS stress are shown in figures 6 and 7. In particular, these figures show the intensity of axial velocity fluctuations and the static pressure for the non-swirling and swirling cases, respectively. Regarding the non-swirling case, the SSM underpredicts the intensity of axial velocity fluctuations at x/D = 1. The SSM does not seem to capture the forcing applied at the inlet of the non-swirling jet flow. Overall, the SSM features are similar to the features of the no-perturbation LES. The three SGS models predict almost the same flow fields for the swirling jet. The features of the DSM and the DKEM are the same for both the swirling and non-swirling cases.

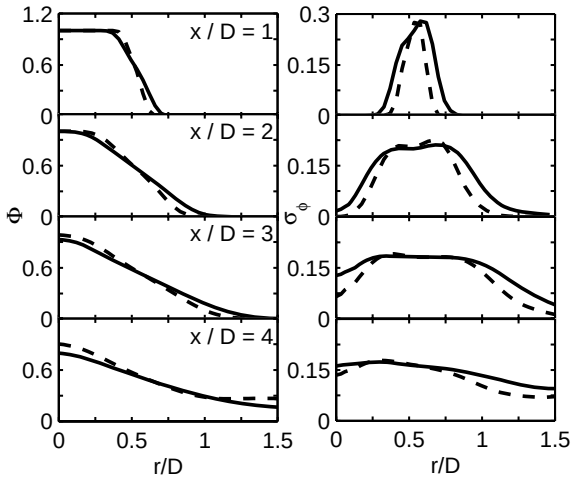

Figure 8: Radial distributions of the averaged scalar Φ and the averaged standard deviation σ_ϕ of the scalar at different axial positions x / D. The solid lines refer to the swirling case and dashed lines refer to the non-swirling case.

Radial distribution of the mean scalar and scalar standard deviation are shown in figure 8. Compared to the swirling case, the mean scalar shows a retarded jet expansion and the scalar standard deviation shows a reduced spreading of the shear layer for the non-swirling case. Hence, the mixing is stronger for the swirling case than for the non-swirling case.

6. SWIRL EFFECTS

After comparing averaged velocity and scalar fields with experimental data [10], instantaneous fields will be analyzed now to explain the effects of swirl. An analysis of instantaneous vorticity distributions was used recently by Mcllwain and Pollard [4] to support the following idea of swirl effects. Ring structures aligned with the plane normal to the flow form downstream of the jet shear layer due to Kelvin-Helmholtz instabilities. The ring structures collide with streamwise braid structures. The resulting interaction causes the ring to break apart into smaller, less organized turbulence structures. The addition of swirl increases the number of streamwise braids, which enhances the breakdown mechanism of the rings. These observations suggest that the increased entrainment observed in swirling flows is due to the action of the braids rather than the rings [4].

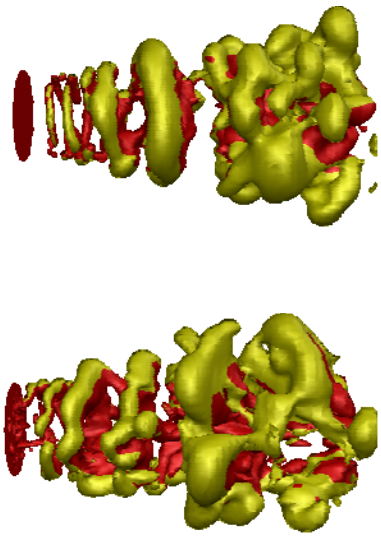

Figure 9: Visualization of coherent vortex structures by means of an iso-surface $\overline{p} - P = -20Pa$ of instantaneous static pressure fluctuations for the non-swirling case (upper picture) and swirling case (lower picture). The iso-surface is colored according to the scalar value: $\overline{\phi} \geq 0.5$ (red) and $\overline{\phi} < 0.5$ (yellow).

Instantaneous vorticity distributions were studied here in accordance to the analysis of Mcllwain and Pollard [4]. It was found, however, that these fields do not represent an appropriate mean to visualize coherent structures: the fields obtained did not reveal ring structures. Most likely, the reason for this finding is given by the fact that Mcllwain and Pollard's sinusoidal forcing was not applied here but the RFG forcing that generates correlated noise: see section 3.

Thus, instantaneous pressure fluctuation fields were considered, which are known to be well appropriate to visualize coherent structures [8, 9]. Figure 9 shows an iso-surface $\overline{p} - P = -20Pa$ of instantaneous static pressure fluctuations for the non-swirling and swirling cases. Here, $\overline{p}$ refers to the filtered pressure and P is the temporally averaged pressure. The iso-surface is colored according to the filtered scalar $\overline{\phi} \geq 0.5$ and $\overline{\phi} < 0.5$. Figure 9 clearly reveals the existence of ring structures (generated by Kelvin-Helmholtz instabilities) and streamwise braid structures. Regarding the swirling case one observes that the streamwise braid structures increase which enhances the breakdown of

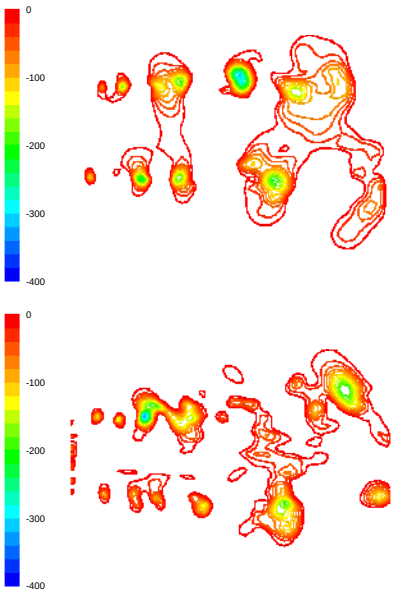

Figure 10: Contour plots of instantaneous static pressure fluctuations $\overline{p} - P$ in Pa for the non-swirling case (upper picture) and the swirling case (lower picture) along the center-plane $z = 0$.

rings. Thus, figure 9 supports Mcllwain and Pollard's notion about the influence of swirl. Figure 10 shows a corresponding contour plot of pressure fluctuations along the center-plane $z = 0$ for the non-swirling and swirling case. Since the pressure inside a vortex or structure will be low compared to the surroundings, these contour plots can be used to identify the location of the large vortices in the flow. In accord with figure 9, figure 10 also indicates the breakdown of ring structures. The consequence of swirl effects for the turbulent mixing of passive scalars is illustrated in figure 11 which shows contour plots of instantaneous scalar values in the center-plane $z = 0$ and in the plane $x = 1D$, respectively. This figure clearly shows the increased mixing efficiency due to the enhanced breakdown of ring structures induced by swirl. The addition of swirl increases the number of streamwise braids, which enhances the breakdown mechanism of ring structures.

7. CONCLUSIONS

RANS and LES methods were combined to simulate swirling and non-swirling turbulent jet flows. In particular, RANS nozzle flow simulations were used to provide inlet profiles for the LES of jet flows. The

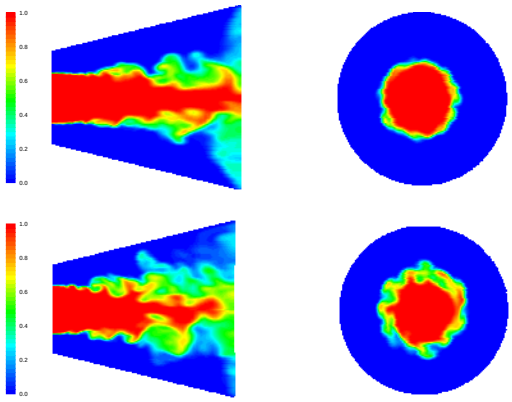

Figure 11: Contour plots of instantaneous scalar values for the non-swirling case (upper pictures) and the swirling case (lower pictures) in the center-plane $z = 0$ (left) and in the plane $x = 1D$ (right).

RFG method of Smirnov et al. [5] was used for the generation of instantaneous LES inflow data. The advantage of this technique is given by the fact that it generates characteristic length and time scales of inflowing instantaneous turbulent eddies which are in consistency with the corresponding RANS profiles imposed at the inlet.

The comparison of averaged flow fields obtained by LES with the experimental data of Gilchrist and Naughton [10] reveals a good agreement. It was shown that the forcing applied clearly has a positive effect. The DSM and DKEM predict almost the same flow fields. These SGS models were found to provide better predictions than the SSM for the non-swirling case. Coherent structures were studied in terms of an analysis of instantaneous flow fields provided by LES. Instantaneous pressure fluctuation fields were found to be most appropriate for the visualization of coherent structures. The results obtained support Mcllwain and Pollard's notion about the influence of swirl. The addition of swirl increases the number of streamwise braids such that the breakdown mechanism of ring structures is enhanced. It was shown that the latter effect increases the intensity of the turbulent mixing of scalars.

ACKNOWLEDGEMENTS

This work has been primarily supported through the Air Force Office of Scientific Research under grant DODAF41603. Dr. John Schmisseur has been the Technical Monitor. The computational resources have

been provided by the Institute of Scientific Computation at the University of Wyoming.

REFERENCES

[1] Farokhi, S., Taghavi, R., and Rice, E., "Modern Developments in Shear Flow Control with Swirl," *AIAA Journal*, Vol. 30, No. 6, 1992, pp. 1482–1483.

[2] Naughton, J. W., Cattafesta, L. N., and Settles, G., "An Experimental Study of Compressible Turbulent Mixing Enhancement in Swirling Jets," *Journal of Fluid Mechanics*, Vol. 330, 1997, pp. 271–305.

[3] Jakirlic, S., Hanjalic, K., and Tropea, C., "Modeling Rotating and Swirling Turbulent Flows: A Perpetual Challenge (review article)," *AIAA Journal*, Vol. 40, No. 10, 2002, pp. 1984–1996.

[4] McIlwain, S. and Pollard, A., "Large Eddy Simulation of the Effects of Mild Swirl on the Near Field of a Round Free Jet," *Physics of Fluids*, Vol. 14, No. 2, 2002, pp. 653–661.

[5] Smirnov, A. and Celik, S. S. I., "Random Flow Generation Technique for Large Eddy Simulations and Particle-Dynamics Modeling," *Journal of Fluids Engineering*, Vol. 123, 2001, pp. 359–371.

[6] Klein, M., Sadiki, A., and Janicka, J., "A Digital Filter Based Generation of Inflow Data for Spatially Developing Direct Numerical or Large Eddy Simulations," *Journal of Computational Physics*, Vol. 186, No. 2, 2003, pp. 652–665.

[7] Bogey, C. and Bailly, C., "Effects of Inflow Conditions and Forcing on Subsonic Jet Flows and Noise," *AIAA Journal*, Vol. 43, No. 5, 2005, pp. 1000–1007.

[8] Garcia-Villalba, M., Frohlich, J., and Rodi, W., "Identification and Analysis of Coherent Structures in the Near Field of a Turbulent Unconfined Annular Swirling Jet Using Large Eddy Simulation," *Physics of Fluids*, Vol. 18, 2006, pp. 1–17.

[9] Frohlich, J., Garcia-Villalba, M., and Rodi, W., "Scalar Mixing and Large-Scale Coherent Structures in a Turbulent Swirling Jet," *Flow, Turbulence and Combustion*, Vol. 80, No. 1, 2008, pp. 47–59.

[10] Gilchrist, R. T. and Naughton, J. W., "Experimental Study of Incompressible Jets with Different Initial Swirl Distributions: Mean Results," *AIAA Journal*, Vol. 43, No. 4, 2005, pp. 741–741.

[11] Mehta, R. D., Wood, D. H., and Clausen, P. D., "Some Effects of Swirl on Turbulent Mixing Layer Development," *Physics of Fluids A*, Vol. 3, No. 11, 1991, pp. 2717–2724.

[12] Germano, M., Piomelli, U., Moin, P., and Cabot, W. H., "A Dynamic Subgrid-Scale Eddy Viscosity Model," *Physics of Fluids*, Vol. 3, No. 7, 1991, pp. 1760–1765.

[13] Smagorinsky, J., "General Circulation Experiments with the Primitive Equations. I. The Basic Experiment," *Monthly Weather Review*, Vol. 91, No. 3, 1963, pp. 99–164.

[14] Kim, W.-W. and Menon, S., "Application of the Localized Dynamic Subgrid-Scale Model to Turbulent Wall-Bounded Flows," *AIAA-97-0210*, 1997.

[15] *FLUENT 6.2 User Guide*, FLUENT INC., Lebanon, NH, 2005.

[16] Heinz, S., "Unified Turbulence Models for LES and RANS, FDF and PDF Simulations," *Theor. Comput. Fluid Dyn*, Vol. 21, No. 2, 2007, pp. 99–118.

[17] Menter, F. R., "Two-Equation Eddy-Viscosity Turbulence Models for Engineering Applications," *AIAA Journal*, Vol. 32, No. 8, 1994, pp. 1598–1605.

[18] Kraichnan, R., "Diffusion by a Random Velocity Field," *Physics of Fluids*, Vol. 13, No. 1, 1970, pp. 245–272.

[19] Mathey, F., Cokljat, D., Bertoglio, J. P., and Sergent, E., "Assessment of the Vortex Method for Large Eddy Simulation Inlet Conditions," *Progress in Computational Fluid Dynamics*, Vol. 6, 2006, pp. 58–67.

[20] Glaze, D. J. and Frankel, S. H., "Stochastic Inlet Conditions for Large-Eddy Simulation of a Fully Turbulent Jet," *AIAA Journal*, Vol. 41, No. 6, 2003, pp. 1064–1073.